Development and performance assessment of an improved 8-node mixed type FEM element

L. Duchêne[1], P. de Montleau[2], A.M. Habraken[2]

[1]*COBO Dept., Royal Military Academy – Avenue de la Renaissance 30, 1000 Brussels, Belgium*
URL: www.cobo.rma.ac.be *e-mail: l.duchene@ulg.ac.be*

[2]*M&S Dept., University of Liège – Chemin des Chevreuils 1, 4000 Liège, Belgium*
URL: www.ulg.ac.be/matstruc *e-mail: anne.habraken@ulg.ac.be*

ABSTRACT: Several finite element (FE) simulations were investigated using a recently developed mixed type element: the BWD3D. The main formulation of the element is largely described, with particular focus on the shear locking treatment. The formulation of the former BLZ3D element is also presented for comparison. The examples investigated in the present study were beam bending, large strain torsion, incremental forming and deep drawing .The numerical results obtained with both elements were compared to experiments.

Key words: finite element, shear locking, hourglass stresses

1 INTRODUCTION

An accurate description of the material's behaviour is required to obtain valuable FE predictions in forming processes. From a numerical point of view, a key point is therefore the yield locus defining the plastic behaviour of the material. The initial yield locus as well as its evolution during plastic deformation must be captured accurately by the constitutive law.
Beside material's model, it appeared that FE formulation has also a large influence on the accuracy of the simulation results. A new FE, named BWD3D, has recently been implemented in the self-made FE code LAGAMINE (developed at M&S department since 1984). In this element name, 'B' stands for Belytschko [1] ; 'W' stands for Wang and Wagoner [2]; 'D' for Duchêne and de Montleau and, finally, '3D' for 3 dimensions. This element is based on the non-linear three-field (stress, strain and displacement) HU-WASHIZU variational principle [1].
Next section is devoted to the description of the BWD3D; the shear locking treatment is mainly focused on. Then, the performance of this element is assessed through beam bending, large strain torsion, incremental forming and deep drawing simulations.
To allow comparison, a former version of LAGAMINE element, called BLZ3D [3], was also tested.

2 BWD3D FORMULATION

A first feature of the BWD3D element is a new shear locking treatment based on the Wang-Wagoner method [2]. This method identifies the hourglass modes responsible of the shear locking and removes them. The second feature of this new element is the use of a corotational reference system, required for the identification of the hourglass modes.
The eight interpolation functions for eight-node solid element are:

$$N_i(\xi,\eta,\zeta)=\frac{1}{8}(1+\xi_i\xi)(1+\eta_i\eta)(1+\zeta_i\zeta) \qquad (1)$$

with $\xi_i,\eta_i,\zeta_i=\pm 1$ and where ξ, η and ζ are the intrinsic coordinates of the element. Rewriting these interpolation functions in matrix form: $\underline{N}_{[24\times 3]}$, interpolation of the velocity field can be obtained:

$$\underline{\dot{u}}=\underline{N}^T\underline{\dot{U}} \quad \text{with} \quad \underline{\dot{u}}=\begin{bmatrix}\dot{u}_x\\ \dot{u}_y\\ \dot{u}_z\end{bmatrix} \quad \text{and} \quad \underline{\dot{U}}=\begin{bmatrix}\underline{\dot{U}}_x\\ \underline{\dot{U}}_y\\ \underline{\dot{U}}_z\end{bmatrix} \qquad (2)$$

$\underline{\dot{U}}_{[24\times 1]}$ is a vector of the nodal velocities and $\underline{\dot{u}}_{[3\times 1]}$ is the interpolated velocity field. Derivation of equation (2) yields to the interpolation of the velocity gradient (expressed in vector form: $\underline{L}_{[9\times 1]}$).

$$\underline{L} = \frac{\partial \underline{\dot{u}}}{\partial \underline{x}} = \frac{\partial \underline{N}^T}{\partial \underline{x}} \underline{\dot{U}} = \underline{B}\underline{\dot{U}} \quad (3)$$

where the velocity gradient interpolation matrix $\underline{B}_{[9\times24]}$ can be expressed in terms of the intrinsic coordinates:

$$\underline{B} = \underline{B}_0 + \xi\underline{B}_\xi + \eta\underline{B}_\eta + \zeta\underline{B}_\zeta + \xi\eta\underline{B}_{\xi\eta} + \xi\zeta\underline{B}_{\xi\zeta} + \eta\zeta\underline{B}_{\eta\zeta} \quad (4)$$

with sub-matrices $\underline{B}_{0[9\times24]}$ and $\underline{B}_{\alpha[9\times24]}$ ($\alpha=\xi,\ \eta,\ \zeta,\ \xi\eta,\ \xi\zeta,\ \eta\zeta$) having the form of equation (5), where $\underline{b}_{i[8\times1]}$ ($i=x,y,z$) are vectors constructed from the nodal coordinates, while $\underline{b}_{i\alpha\,[8\times1]}$ vectors are function of the intrinsic coordinates ξ,η,ζ and depend on the nodal coordinates.

$$\underline{B}_0 = \begin{bmatrix} \underline{b}_x^T & \underline{0} & \underline{0} \\ \underline{b}_y^T & \underline{0} & \underline{0} \\ \underline{b}_z^T & \underline{0} & \underline{0} \\ \underline{0} & \underline{b}_x^T & \underline{0} \\ \underline{0} & \underline{b}_y^T & \underline{0} \\ \underline{0} & \underline{b}_z^T & \underline{0} \\ \underline{0} & \underline{0} & \underline{b}_x^T \\ \underline{0} & \underline{0} & \underline{b}_y^T \\ \underline{0} & \underline{0} & \underline{b}_z^T \end{bmatrix}, \underline{B}_\alpha = \begin{bmatrix} \underline{b}_{x\alpha}^T & \underline{0} & \underline{0} \\ \underline{b}_{y\alpha}^T & \underline{0} & \underline{0} \\ \underline{b}_{z\alpha}^T & \underline{0} & \underline{0} \\ \underline{0} & \underline{b}_{x\alpha}^T & \underline{0} \\ \underline{0} & \underline{b}_{y\alpha}^T & \underline{0} \\ \underline{0} & \underline{b}_{z\alpha}^T & \underline{0} \\ \underline{0} & \underline{0} & \underline{b}_{x\alpha}^T \\ \underline{0} & \underline{0} & \underline{b}_{y\alpha}^T \\ \underline{0} & \underline{0} & \underline{b}_{z\alpha}^T \end{bmatrix} \quad (5)$$

The BWD3D element is defined with only one integration point (IP). So, evaluation of the velocity gradient at the IP induces that the interpolation matrix $\underline{B}$ reduces to $\underline{B}_0$, because the IP is located at the centre of the element ($\xi=\eta=\zeta=0$). This consideration yields to the existence of twelve non-zero deformation modes $\underline{\dot{U}}$ corresponding to a velocity gradient $\underline{L}$ equal to zero at the IP. These are the so-called hourglass modes: 6 bending modes, 3 torsion modes and 3 warp (non-physical) modes (see figure 1).

Stress computed at the IP corresponding to hourglass modes is zero (because $\underline{L}=\underline{0}$). Without particular care, the deformation energy associated to hourglass modes would be zero. No stiffness of the element with respect to hourglass deformation modes would derive.

Gratefully, an estimation of the stress field inside the element can be obtained using the tangent stiffness matrix $\underline{C}_{[9\times9]}$ as shown by equation (6), where $\underline{\dot{\sigma}}_{[9\times1]}$ is the stress field expressed in vector form, $\underline{\dot{\sigma}}_0$ is the stress at IP and $\underline{\dot{\sigma}}_\xi$, $\underline{\dot{\sigma}}_\eta$, $\underline{\dot{\sigma}}_\zeta$, $\underline{\dot{\sigma}}_{\xi\eta}$, $\underline{\dot{\sigma}}_{\xi\zeta}$, $\underline{\dot{\sigma}}_{\eta\zeta}$ are the six so-called hourglass stresses. Note that, according to the FE time integration, the derivative of the stress with respect to time is actually computed.

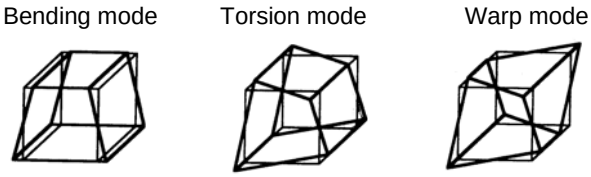

Fig. 1. Hourglass mode types

$$\begin{aligned} \underline{\dot{\sigma}} &= \underline{C}\underline{L} \\ &= \underline{C}\left[\underline{B}_0 + \xi\underline{B}_\xi + \eta\underline{B}_\eta + \zeta\underline{B}_\zeta + \xi\eta\underline{B}_{\xi\eta} + \xi\zeta\underline{B}_{\xi\zeta} + \eta\zeta\underline{B}_{\eta\zeta}\right]\underline{\dot{U}} \\ &= \underline{\dot{\sigma}}_0 + \xi\underline{\dot{\sigma}}_\xi + \eta\underline{\dot{\sigma}}_\eta + \zeta\underline{\dot{\sigma}}_\zeta + \xi\eta\underline{\dot{\sigma}}_{\xi\eta} + \xi\zeta\underline{\dot{\sigma}}_{\xi\zeta} + \eta\zeta\underline{\dot{\sigma}}_{\eta\zeta} \end{aligned} \quad (6)$$

With this stress field and the velocity gradient inside the element (equation (3)), a non-zero deformation energy can be attributed to hourglass modes.

However, it is generally admitted that the energy computed thanks to the hourglass stresses is too high, depending on the deformation mode applied to the element. Consequently, the element is sometimes too stiff. This problem is known as locking phenomenon. A simple method, used in the BLZ3D element, to avoid locking is to replace $\underline{B}$ matrix by $\overline{\underline{B}}_{[9\times24]}$ matrix:

$$\overline{\underline{B}} = \underline{B}_0 + \xi\overline{\underline{B}}_\xi + \eta\overline{\underline{B}}_\eta + \zeta\overline{\underline{B}}_\zeta + \xi\eta\overline{\underline{B}}_{\xi\eta} + \xi\zeta\overline{\underline{B}}_{\xi\zeta} + \eta\zeta\overline{\underline{B}}_{\eta\zeta} \quad (7)$$

Where $\underline{B}_0$ is identical as in equation (4), while the $\overline{\underline{B}}_{\alpha\,[9\times24]}$ matrices have the form of equation (8), where e_1, e_2 and e_3 are parameters used to avoid volumetric locking, i.e. locking problem occurring during volumetric deformation. Parameter β is introduced to reduce shear locking (linked to shear strains).

$$\overline{\underline{B}}_\alpha = \begin{bmatrix} e_1\underline{b}_{x\alpha}^T & e_3\underline{b}_{y\alpha}^T & e_2\underline{b}_{z\alpha}^T \\ \beta\underline{b}_{y\alpha}^T & \underline{0} & \underline{0} \\ \beta\underline{b}_{z\alpha}^T & \underline{0} & \underline{0} \\ \underline{0} & \beta\underline{b}_{x\alpha}^T & \underline{0} \\ e_2\underline{b}_{x\alpha}^T & e_1\underline{b}_{y\alpha}^T & e_3\underline{b}_{z\alpha}^T \\ \underline{0} & \beta\underline{b}_{z\alpha}^T & \underline{0} \\ \underline{0} & \underline{0} & \beta\underline{b}_{x\alpha}^T \\ \underline{0} & \underline{0} & \beta\underline{b}_{y\alpha}^T \\ e_3\underline{b}_{x\alpha}^T & e_2\underline{b}_{y\alpha}^T & e_1\underline{b}_{z\alpha}^T \end{bmatrix} \quad (8)$$

The volumetric locking can be completely eliminated by choosing $e_1=2/3$ and $e_2=e_3=-1/3$. Unfortunately, the shear locking cannot be treated as simply. The value of β ($\in[0,1]$) should be adapted to the deformation mode applied to the element: a value near 0 is recommended for bending dominated problems to avoid shear locking while a value around 1 should be used during shearing of the element to avoid hourglass modes without

deformation energy.
The main drawbacks of the shear locking method proposed by equations (7) and (8) are the dependence of the optimum β-value on the deformation undergone by the element. To facilitate the determination of β, some authors propose to approximate the deformation mode dependence by a dependence on the element shape [4]. A second drawback is the non-objectivity of the $\underline{\overline{B}}$ matrix, i.e. dependence of the element behaviour on the global reference axes. This second drawback can hardly be avoided.
These considerations led us to the development of a new locking treatment method: the Wang-Wagoner method [2], implemented in the BWD3D element. To do so, equations (3) and (4) are adapted in order to express the velocity gradient in term of hourglass modes:

$$\frac{\partial \dot{u}_i}{\partial x_j} = \left(\underline{b}_j^T + \frac{\partial h_1}{\partial x_j}\underline{\gamma}_1^T + \frac{\partial h_2}{\partial x_j}\underline{\gamma}_2^T + \frac{\partial h_3}{\partial x_j}\underline{\gamma}_3^T + \frac{\partial h_4}{\partial x_j}\underline{\gamma}_4^T \right) \underline{\dot{U}}_i \quad (9)$$

with $h_1 = \eta\zeta; h_2 = \xi\zeta; h_3 = \xi\eta; h_4 = \xi\eta\zeta$

In equation (9), the first term $\underline{b}_{j[8\times1]}$ corresponds to uniform shear (if $i \neq j$) or uniform tension (if $i=j$), while $\underline{\gamma}_{1[8\times1]}$, $\underline{\gamma}_{2[8\times1]}$, $\underline{\gamma}_{3[8\times1]}$, $\underline{\gamma}_{4[8\times1]}$ are linked to four hourglass modes: two bending modes, one torsion mode and one warp mode (the twelve hourglass modes are recovered for i=1,2,3).
According to [2], locking problems can be avoided by eliminating adequate hourglass modes. For shear locking, the uniform shear and the hourglass torsion modes must be kept while the two bending and the warp modes are identified to be at the origin of shear locking; therefore, they should be eliminated. Equation (9) is modified into equation (10) for $i \neq j$:

$$\frac{\partial \dot{u}_i}{\partial x_j} = \left(\underline{b}_j^T + \frac{\partial h_i}{\partial x_j}\underline{\gamma}_i^T \right) \underline{\dot{U}}_i \qquad (i \neq j \text{; no sum on } i) \qquad (10)$$

To prevent volumetric locking, equation (9) becomes equation (11) in order to eliminate the dilatational strain caused by torsion, bending and warp hourglass modes.

$$\begin{aligned} \frac{\partial \dot{u}_i}{\partial x_j} = & \left(\underline{b}_j^T + \frac{2}{3}\left[\frac{\partial h_k}{\partial x_j}\underline{\gamma}_k^T + \frac{\partial h_l}{\partial x_j}\underline{\gamma}_l^T + \frac{\partial h_4}{\partial x_j}\underline{\gamma}_4^T \right] \right) \underline{\dot{U}}_i \\ & -\frac{1}{3}\left(\frac{\partial h_l}{\partial x_k}\underline{\gamma}_i^T + \frac{\partial h_l}{\partial x_k}\underline{\gamma}_l^T + \frac{\partial h_4}{\partial x_k}\underline{\gamma}_4^T \right) \underline{\dot{U}}_k \\ & -\frac{1}{3}\left(\frac{\partial h_l}{\partial x_l}\underline{\gamma}_i^T + \frac{\partial h_k}{\partial x_l}\underline{\gamma}_k^T + \frac{\partial h_4}{\partial x_l}\underline{\gamma}_4^T \right) \underline{\dot{U}}_l \end{aligned} \qquad (11)$$

$(i = j;\ \ i \neq k \neq l;\ \ i,k,l = 1,2,3$; no sum on $i,k,l)$

In order to be able to identify the hourglass modes (which is a crucial point of the method), equation (9) must be expressed in a corotational reference system [1], closely linked to the element coordinates. This reference system must have its origin at element centre and its reference axes are aligned (as much as possible, depending on the element shape) with element edges. A grateful consequence of this corotational reference system is a simple and accurate treatment of the hourglass stress objectivity, by using initial and final time step rotation matrices.
The shear and volumetric locking method proposed by equations (10) and (11) associated with the corotational reference system has been successfully implemented in the BWD3D element of LAGAMINE FE code. The Wang-Wagoner method, contrarily to the method using a β parameter (equation (8)), has deep physical roots, which makes it very efficient for various FE analyses.

3 APPLICATIONS

In this section, the superiority of the BWD3D element compared with elements having a shear locking treatment using a β parameter (BLZ3D element) is shown through one small-scale academic problem and three actual deformation processes.

3.1 Beam bending

An elastic cantilever beam was subjected to an end shear force (see figure 2). This linear deformation mode was modelled with three elements in the thickness. Five different element aspect ratios were tested and the relative errors with analytical solutions are shown in table 1 for BWD3D and BLZ3D elements.
The errors for the BWD3D element were in the range 3.7% to 3.9%, i.e. a very low dependence on the element aspect ratio. The results obtained with the BLZ3D element were more accurate but an appropriate β value must be chosen (see table 1).

Table1. Relative error on tip deflection for beam bending

Aspect ratio		1	2	4	6	8
BLZ3D		3.6 %	3.05 %	1.01 %	0.34 %	0 %
	β	0.2	0.2	0.196	0.147	0.1162
BWD3D		3.9 %	3.87 %	3.82 %	3.74 %	3.78 %

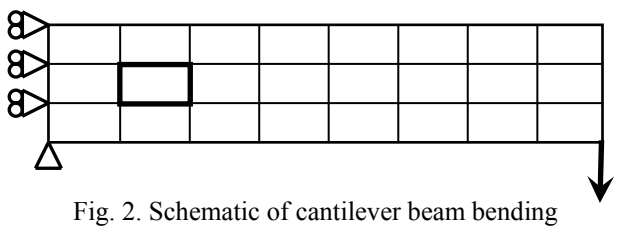

Fig. 2. Schematic of cantilever beam bending

3.2 Large strain torsion

The free-end torsion of copper bars was simulated with the BWD3D and the BLZ3D elements. The material's behaviour was modelled with a micro-macro constitutive law taking into account texture evolution [5]. Further details about experimental procedure can be found in [6] while the numerical simulations are described in [7].
The axial lengthening of the cylinder, i.e. the so-called Swift effect, is plotted as a function of the shear strain in figure 3. According to figure 3, it appears that the results obtained with the BLZ3D element are satisfactory, compared to experimental results, for shear strain up to around 0.3, while the BWD3D remains accurate for shear strain up to 1.0.

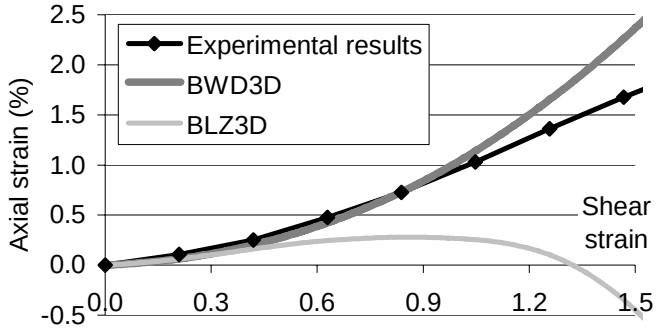

Fig. 3. Axial strain versus shear strain during free-end torsion (experimental results from [6])

3.3 Incremental forming

Sheet metal forming process was analysed through incremental forming of one cone with a hemispherical tool. The tool displacement during the process, corresponding to successive circular paths at increasing depth, is represented in figure 4. More details about the process can be found in [8].

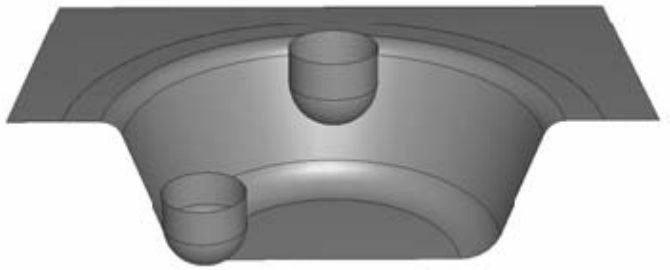

Fig. 4. Schematic of cone incremental forming

Fig. 5. Metal sheet profile during incremental forming with BLZ3D elements (a) and BWD3D elements (b)

At the beginning of the simulation, both element types behaved correctly. But, progressively, the metal sheet profile predicted using BLZ3D elements became completely inaccurate compared to experimental observations (figure 5). On the other hand, the sheet profile predicted by BWD3D elements remained correct during the whole process.

3.4 Deep drawing

In the BLZ3D formulation (equation (8)), the non-objectivity of hourglass stresses influences inappropriately the earing profile prediction during deep drawing simulations. Contrarily, very accurate earing profile predictions were obtained with the BWD3D element (see [9]).

4 CONCLUSIONS

The four numerical simulations presented in this paper prove the superiority of the recently developed BWD3D element compared to its former version: the BLZ3D element.

ACKNOWLEDGEMENTS

A.M. Habraken is mandated by the National Fund for Scientific Research (Belgium). The authors thank the Belgian Federal Science Policy Office (Contract P5/08) for its financial support.

REFERENCES

1. T. Belytschko and L.P. Bindeman, *Comput. Methods Appl. Mech. Engrg*. 88 (1991) 311-340.
2. J. Wang and R.H. Wagoner, A New Hexahedral Solid Element for 3D FEM Simulation of Sheet Metal Forming, In *Proc. NUMIFORM*, eds, S. Ghosh et al., AIP Conf. Proc. 712 (2004) 2181-2186.
3. Y.Y. Zhu and S. Cescotto, Transient thermal and thermomechanical analysis by F.E.M. *Computers and Structures* 53(2) (1994) 275-304.
4. K.P. Li and S. Cescotto, *Comput. Methods Appl. Mech. Engrg.* 141 (1997) 157-204.
5. A.M. Habraken and L. Duchêne, *Int. J. Plast.* 20 (2004) 1525-1560.
6. L.S. Toth, J.J. Jonas, D. Daniel and J.A. Bailey, Texture development and length changes in copper bars subjected to free end torsion. *Textures and Microstructures* 19 (1992) 245-262.
7. L. Duchêne, F. El Houdaigui, A.M. Habraken, Finite element simulations of the Swift effect, In: *Proc. ICTP 2005*, ed, P.F. Bariani.
8. C. Henrard, Development of a contact model adapted to incremental forming, *DEA Graduation Work*, University of Liège, Belgium, sept. 2005.
9. L. Duchêne, P. de Montleau, F. El Houdaigui, S. Bouvier, A.M. Habraken, Analysis of texture evolution and hardening behavior during deep drawing with an improved mixed type FEM element, In: *NUMISHEET*, eds, L.M. Smith et al., AIP Conf. Proc. 778 (2005) 409-414.